Journal of Applied Polymer Science

Study the effects of Cloisite15A nanoclay incorporation on the morphology and gas permeation properties of Pebax2533 polymer

Maryam Behroozi, Majid Pakizeh
Department of Chemical Engineering, Faculty of Engineering, Ferdowsi University of Mashhad, P.O. Box 9177948974, Mashhad, Iran
Correspondence to: M. Pakizeh (E-mail: pakizeh@um.ac.ir)

ABSTRACT: In this study, mixed matrix membranes (MMMs) were prepared using commercially available poly(ether-*b*-amide) (Pebax2533) as polymer matrix and organically modified montmorillonite (OMMt) as filler with the aim of investigating their gas permeation properties. The prepared membranes were characterized by Fourier-transform infrared (FTIR) spectroscopy, X-ray diffraction (XRD), scanning electron microscope (SEM), thermal gravimetric analysis, and tensile strength analyses. Gas permeation properties of all the prepared membranes were evaluated at different pressures and clay loadings. Results of FTIR and SEM confirmed the appropriate adhesion between polymer and nanoclays so that no void formation was observed in the polymer/clay interface. XRD results showed that in low loading, clay dispersion occurred as exfoliated-intercalated and at high loading as intercalated-phase separated. Results of gas permeation test showed that by adding layered and impermeable clay particles to the polymer matrix, the permeation of soluble CO_2 gas reduced by 28% for the highest clay loading. By increasing of pressure from 2 to 6 bar, CO_2/CH_4 permselectivity increased at all nanoclay loadings. The highest CO_2/CH_4 selectivity was obtained for 6 wt % clay MMM at all pressures, while the highest CO_2/H_2 selectivity was achieved for neat polymer at 6 bar. © 2017 Wiley Periodicals, Inc. J. Appl. Polym. Sci. **2017**, *134*, 45302.

KEYWORDS: gas permeation; mixed matrix membrane; nanoclay; OMMt; Pebax 2533

Received 3 December 2016; accepted 21 April 2017
DOI: 10.1002/app.45302

INTRODUCTION

Traditional processes such as physical absorption, reactive absorption, solid bed adsorption,[1] cryogenic distillation, and pressure swing adsorption (PSA) have been employed for industrial gas separation.[2] Membrane-based gas separation is a more efficient and environmental friendly process which has attracted much efforts.[1] The main part of a membrane process is the membrane itself[3] that can be made of polymeric or inorganic materials. Polymeric membranes have some advantages such as processability, intrinsic transport properties, low cost,[1,3] good thermostability, and high energy efficiency.[4] However, there is a trade-off limitation between gas permeability and selectivity demonstrated as the Robeson upper-bound relationship.[1,4] On the other hand, inorganic materials have appropriate thermal and chemical stabilities and high gas separation ability even in hard operating conditions.[3,5] However using this materials is still limited because of their fragility problems in the preparation or application steps, short lifetime, and high cost.[3,6] To improve the overall membrane effectiveness and prevailing these problems, organic and inorganic materials can be used together, leading to the fabrication of mixed matrix membranes (MMMs).[5,7] A MMM consists of an inorganic phase dispersed in a continuous polymeric phase. On the other hand, the concept of MMM combines the advantages of two mentioned phases: high selectivity of the dispersed particles, desirable mechanical properties and economical processability of the polymers matrix.[3,7–9] The organic fillers used in the literature include porous particles such as carbon molecular sieves, zeolites, metal organic frameworks (MOF), activated carbons, carbon nanotubes (CNT), metal oxides nanoparticles, and nonporous particles such as silicalites and clays,[3,4,6,10] etc. However, polymer/clay MMMs have attracted a great interest of researchers due to proper properties including, mechanical properties and gas barrier properties, thermal stability, biodegradability,[9] and high gas separation performance[7,11] when compared to neat polymers.

Clay minerals are defined as natural, earthy, fine-grained materials which are generally plastic at appropriate amount of water.[3,11] Clay minerals are generally classified into three major groups: Kaolinite, Smectite, and Illite or Mica as shown in Table I.[11] Among these major groups, smectite types, or particularly montmorillonite (Mt), have received specific attention

Table I. Classification of Clay Mineral

Clay group	Main members	Chemical formula
Kaolinite group	Kaolinite	$Al_2Si_2O_5(OH)_4$
	Dickite	
	Nacrite	
Smectite group	Vermiculate	(Ca, Na, H) (Al, Mg, Fe, Zn)$_2$ (Si, Al)$_4O_{10}(OH)_2$-xH_2O
	Saponite	
	Hectorite	
	montmorillonite	
	talc	
	Sauconite	
	Nontronite	
Illite or mica-clay group	Muscovites	(K, H)Al_2(Si, Al)$_4$ $O_{10}(OH)_2$-xH_2O

due to their suitable dispersion in the polymer matrix, high specific surface area (up to 750–800 m^2/g), low cost, non-toxicity, availability, and abundance in nature.[11,12] Mt is a member of phyllosilicates group that have 2:1 layered or plate-like structure. In this structure, the two tetrahedral mineral silica sheets, having an octahedral alumina sheet inside them, are bound with van der Waals forces. The thickness of silicate layer is around 1 nm, and the lateral dimensions may vary in range of 30 nm to several micrometers or even larger, depending on the particular layered silicate.[7,11] The distance between specific layers are called interlayer that are occupied by cations such as Li^+, Na^+, Rb^+, and Cs. By changing the cations with another functional groups including primary, secondary, tertiary, and quaternary alkyl ammonium or alkyl phosphonium, the hydrophilicity nature of this materials will be changed to hydrophobicity, making it possible to use them with a large range of hydrophobic engineering polymers which will increase dispersion and compatibility.[11] Depending on the strength of polymer–silicate interaction, three main morphologies are possible in clay polymer nanocomposites: phase separated, intercalated, or exfoliated,[7,12–14] as shown in Figure 1. The resulted structure of the polymer/clay nanocomposite is affected by factors such as: organic modification of the clay, the amount of modifier, the organic modifier polarity, polymer type, and synthesis techniques.[14] Phase separated structure occurs due to the limited incorporation of polymer chain into the clay galleries.[7,14]

In intercalated structure, polymer chains are inserted into the clay interlayer space resulting in weaker layers interaction. Hence this gap becomes expanded.[7,12,14,15] For the case of exfoliated structure, the individual clay layers are dispersed randomly into the continuous polymer due to over much penetration of polymer molecules.[7,12,14]

Effects of clay loading on morphology and gas separation properties of various polymer matrixes such as: polyetherimide (PEI),[3] polysulfone (PSf),[7] polyethersulfone,[4,10] polyvinylidene,[6] poly(ethylene-*co*-vinyl acetate),[8] polypropylene,[16] polydimethylsiloxane[17] were investigated.

Hashemifard *et al.*,[3] used five different industrially functionalized Mt nanoclays as filler in PEI matrix. Cloisite15A was recognized as the most prominent among the five clays for CO_2/CH_4 separation. They concluded that for loading of 0.5 wt % Cloisite15A, optimum selectivity (28% enhancement) is achieved due to perfect adhesion between the organic–inorganic phases. However, beyond 1 wt % loading, due to the increase in clay agglomeration, an explicit reduction in selectivity was observed. Zulhairun *et al.*[7] found that the inserting of low loading of Coisite15A particles in the PSf matrix has led to considerable increment in the gas permeance. The phase separated clay structure was believed to be responsible for the increase in the overall gas permeance and decrease in permeselectivity. Although most of prominent MMMs have been prepared from glassy polymers, rubbery polymers usually offer higher permeability. In addition, rubbery polymers have good interaction with fillers due to more chain mobility; consequently, defect-free MMMs will be more achievable by using rubbery polymers.[18] Pebax2533 is a member of copolymers which contains 80 wt % soft poly(tetra methylene oxide) (PTMO) and 20 wt % rigid polyamide (PA12, nylon-12) and has great mechanical properties.[18–20] So that this copolymer is a fine choice of membrane material for the continuous phase for gas separation. As well as Cloisite15A that has

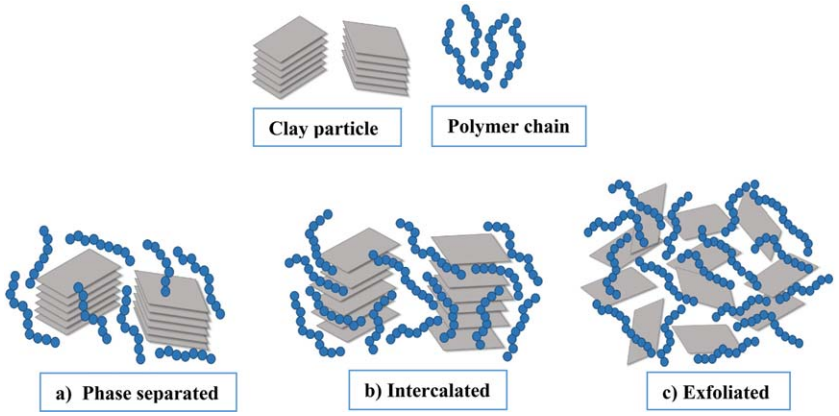

Figure 1. Clay dispersion modes: (a) phase separated, (b) intercalated, (c) exfoliated. [Color figure can be viewed at wileyonlinelibrary.com]

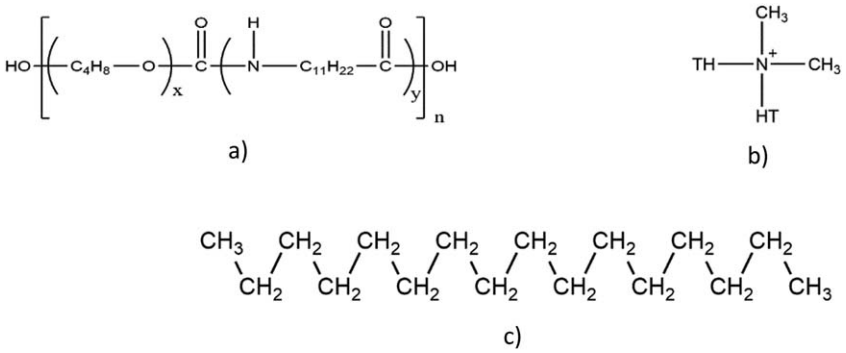

Figure 2. Chemical structure of (a) Pebax2533, (b) dimethyl dehydrogenated tallow ammonium (clay modifier), (c) HT.

attracted much attention among clay families due to its modification by quaternary ammonium functional group resulting in more polymer–clay interfacial adhesion. In this study, Cloisite15A nanoplates as nanofillers were blended with Pebax2533 as support for membrane samples. To the best knowledge of the authors, this is the first report on MMM using Pebax2533/Cloisite15A nanocomposite for gas separation applications. One of the objectives of this study is to investigate the effect of the loading of Cloisite15A nanoplates on the structural characteristics and separation properties of prepared MMM. Another objective is to estimate ability of this new MMM for separation of CO_2 from other gases. Analyses methods including, tensile strength, X-ray diffraction (XRD), Fourier-transform infrared spectroscopy (FTIR), scanning electron microscope (SEM), and thermal gravimetric analysis (TGA) were used for characterization.

EXPERIMENTAL

Materials

Polyether block amid (Pebax2533), that was used as the basic polymer for the preparation of the dense nanocomposite membrane, is a block copolymer contain 80 wt % PTMO and 20 wt % polyamide (PA12, nylon-12), and was provided by Arkema (France). The inorganic filler, organically modified montmorillonite (OMMT), known with the trade name Cloisite15A, with a cation exchange capacity of 1.2 meq/g (modifier concentration), was purchased by Southern Clay Products Inc. Gonzales, TX, and H_2, N_2, CH_4, and CO_2 gases ($\geq$99.99%) were obtained from Technical Gas Services. Also ethanol, supplied by Merck (Billerica, MA) was used as solvent. Pebax2533 pellet and Cloisite15A powder were preconditioned in an oven at 120 °C for at least 72 h to remove trapped moisture. The general chemical formula of Pebax2533 and OMMT modifier are given in Figure 2.

MMM Preparation

Pebax2533 was prepared as a defect-free dense flat membrane by the solvent evaporation method. Ethanol was used to make an 8 wt % Pebax2533 solution. The polymer was dissolved under reflux condition and magnetically stirred continuously at 90 °C for 2–3 h. After the polymer was completely dissolved, it was sonicated for 5 min to eliminate trapped air bubbles. The polymer solution was then cooled to ambient temperature with a slight stirring resulting in a homogeneous solution without gelation. The dense membrane of pure Pebax2533 was obtained by casting 8 wt % polymer solution on a glass petri dish. For preparing the MMMs solutions, the desired amount of clay powder was carefully added to the solvent and the suspension was stirred for 15 min in ambient temperature before being sonicated for 30 min at 40 °C, to obtain maximum dispersion. To obtain optimum wetting of Coisite15A particles, the filler was first subjected to priming upon the addition of 15 wt % of the total polymer and agitated for at least 2–3 h. Subsequently, the remaining polymer was gradually added to the solution and stirred until complete dissolution of the polymer was achieved. The homogenous solution was finally sonicated for 15 min at 40 °C prior to be degased and to ensure a complete dispersion of particles.

The solution was then poured on a glass petri dish and allowed the solvent to evaporate. The casted membrane was dried at room temperature for one day in a saturated media and one day in a semi-saturated media in order to control the rate of solvent evaporation, then the membranes were left to dry at room conditions for another 24 h. After being detached from the glass plate, by immersing the membrane together with the glass plate into distillated water, all the resulted membranes further were placed in an oven at 80 °C temperature for 24 h, in order to guarantee a complete removal of the residual solvent. Pebax2533/cloisite15A flat sheet MMM with area of 12 cm^2 were then used for single gas permeation test in a constant pressure setup.[19] The thickness of prepared membranes was measured by a digital micrometer and varied between 100 and 120 μm.

Membrane Characterization

Fourier-Transform Infrared Spectroscopy. FTIR spectra of the samples were recorded on a Thermo Nicolet Avatar 370 spectrophotometer (USA) with a resolution of 4 cm^{-1}. All FTIR spectra were presented at wavenumbers in the range of 500–4000 cm^{-1}.

X-ray Diffraction. The dispersion of layered silicate in the polymer/clay nanocomposite membranes was determined using XRD (Philips Analytical X-ray, PW1800, using CuKα as the source of radiation at acceleration voltage of 40 kV and current of 30 mA). The diffraction curves were obtained in the scanning range of 2θ between 4° and 60° at a scanning speed of 0.02°/s.

Surface Morphology. The surface and cross-section morphology of neat and Pebax2533/Cloisite15A MMM were observed using

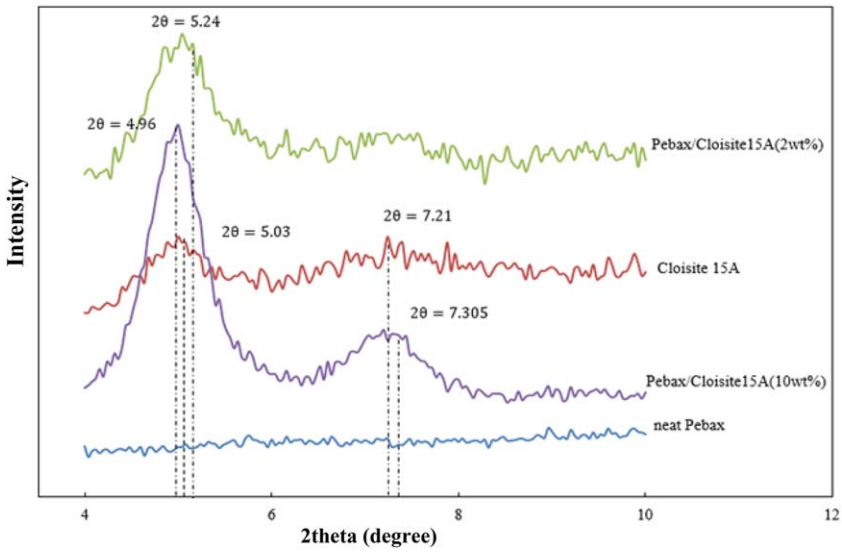

Figure 3. XRD pattern for Cloisite15A, neat Pebax2533, and MMM membranes. [Color figure can be viewed at wileyonlinelibrary.com]

a SEM (LED 1450 VP, Germany). To achieve a clean cut for the cross-sectional view, small pieces of membranes samples were fractured in liquid nitrogen. Then, all the samples were gold-coated by sputtering to produce electrical conductivity and to avoid the electrostatic charge dissipation. In addition, the morphology of clay powder was observed by a field emission scanning electron microscope (FESEM: MIRA3 TESCAN, Czech). To obtain a clear picture of the particles, a mixture of clay powder in solvent was deeply stirred by the probe device for 30 min.

Mechanical Properties. Tensile test was carried out at room temperature on a SANTAM-STM20 tensile testing machine (Iran). The mechanical properties of the nanocomposite membranes including: elongation at break and tensile strength values were measured with a crosshead speed of 40 mm/min. For this purpose, the samples were cut in size of 70 mm × 10 mm. At least three measurements were carried out for each sample and the average value and standard deviation of tensile strength are reported.

Thermogravimetric Analysis. TGA analysis was used to measure mass loss as a function of temperature, to investigate the degradation of the composites, and thus the thermal stability of the specimens. The experiment was performed on both the neat Pebax2533 membrane and MMMs using TGA50-SHIMADZU (Japan). Samples were heated from 25 to 1000 °C at a heating rate of 10 °C/min and under air atmosphere with an air flow rate of 20 mL/min.

Gas Permeability and Selectivity. Single gas permeation properties of the prepared membranes were determined by using a constant pressure/variable volume method.[18,19] The permeation tests were carried out at 25 °C and feed side pressures of 2, 4, and 6 bar. The gas permeation rate through the membranes was measured with a bubble flow meter and repeated three times for each membrane. Gas permeation test was continued for each gas until steady state flow was reached and conducted in a permeation cell with an effective membrane area of 12 cm^2. The gas permeance and selectivity were calculated as follows:

$$q_{lab} = \Delta V / t \quad (1)$$

$$(pq/T)_{lab} = (pq/T)_{STP} \quad (2)$$

$$j = q_{STP} / A_m \quad (3)$$

$$Q = j/\Delta p = P/l_m \quad (4)$$

$$P = Q \times l_m \quad (5)$$

where, q_{lab} and $(T,P)_{lab}$ are laboratory gas flow rate $\left(\frac{cm^3}{s}\right)$, temperature and pressure, respectively. Also standard gas flow rate, $q_{STP}\left(\frac{cm^3 STP}{s}\right)$, can be calculated according to standard temperature and pressure, $(T,P)_{STP}$. Thereafter flux $\left[J\left(\frac{cm^3 STP}{s \cdot cm^2}\right)\right]$ and permeance $\left[Q\left(\frac{cm^3 STP}{cm\ Hg \cdot s \cdot cm^2}\right)\right]$ can be determined. Finally by using the membrane effective thickness $[l_m(m)]$ and area $[A_m(m^2)]$ the gas permeability can be calculated in unit of Barrer (1 Barrer $= 10^{-10} \frac{cm \cdot cm^3 STP}{cmHg \cdot s \cdot cm^2}$).

RESULTS AND DISCUSSION

XRD Analysis

The XRD patterns of pure Pebax, Cloisite15A, and Pebax/Cloisite15A nanocomposite membranes (2, 10 wt %) are shown in Figure 3. The XRD pattern of the Cloisite15A particles exhibited two well-defined reflection at $2\theta = 5.03°$ and $2\theta = 7.21°$, corresponding to $d001$ and $d002$ planes, respectively. The first reflection is associated with the reflections at planes (001) which correspond to basal distance of this plane (17.554 Å according to the Bragg's law). The second reflection shows the presence of the tallow molecules which are incorporated into the clay interlayers.[10,12,21] Neat Pebax2533 spectrum show no obvious reflection below $2\theta = 10°$ while, MMMs exhibit new reflection below $2\theta = 6°$ which indicates the presence of clay particles.[7]

For MMM (2 wt %) sample, the crystalline reflection at $2\theta = 7.1°$ was broader than that of pure Cloisite15A. It can be concluded that partial exfoliated composite membrane is obtained at low loading.[12,21] In contrast, in MMM (10 wt %) sample, the two crystalline reflections are observed at $2\theta = 4.96°$

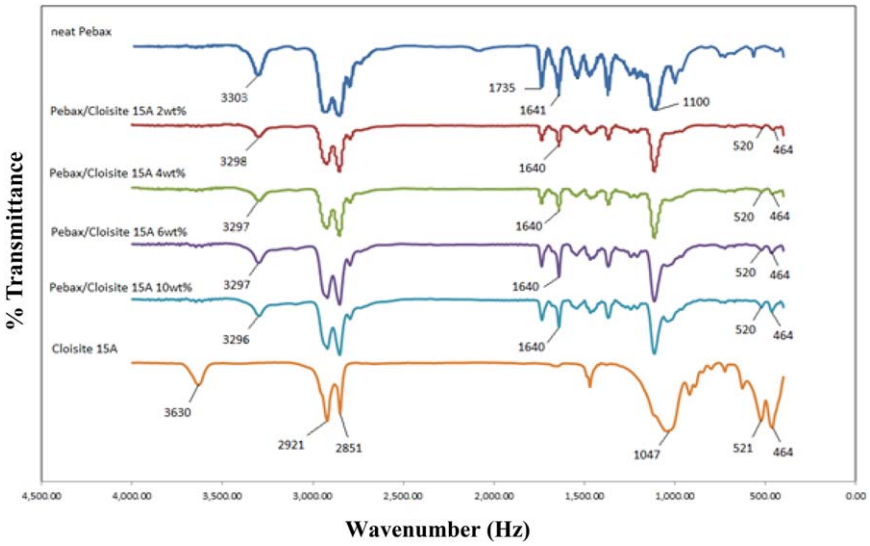

Figure 4. FTIR spectra for Cloisite15A, Pebax2533, and MMMs. [Color figure can be viewed at wileyonlinelibrary.com]

and $2\theta = 7.305°$, the former is shifted to a bit lower angle compared to Cloisite15A. In this case, it can be said that Cloisite15A layers are intercalated within the Pebax matrix but the expansion of the clay layers are too small to be accredited to polymer intercalation inside the silicate layers. Therefore, the Pebax2533–clay combination formed intercalated/phase separated composite rather than intercalated/exfoliated nanocomposite at higher loadings.[7]

FTIR Analysis

To investigate the polymer–clay interaction, structural characteristics bands were evaluated by FTIR. The spectra of the Pebax2533, Cloisite15A, and Pebax2533/Cloisite15A MMMs are presented in Figure 4. The Structural characteristics bands of Pebax2533 are: the strong band at 3300 cm^{-1} is attributed to N—H stretching in amine group of polyamide block,[22,23] other peak at 1640 cm^{-1} indicates the stretching vibration of the H—N—C=O group. Also two absorption bands that have overlapped at 1735 and 1100 cm^{-1} in Pebax are attributed to the C=O and C—O stretching vibrations, respectively.[22–24]

The spectrum of Cloisite15A nanoplates exhibits a characteristic band at 3630 cm^{-1}, due to the stretching vibrations of structural OH groups coordinated to Al–Al pairs.[12,25,26] The sharp bands around 2922 and 2851 cm^{-1} indicate the C—H stretching and bending, respectively. In addition, bands observed at 1047, 464, 627, and 523 cm^{-1} are related to asymmetric Si—O stretching, asymmetric N—H stretching vibration, and Si—O—Al vibration, respectively.[12,26] The FTIR spectrum of the MMMs shows an extra band at 464 cm^{-1} compared to neat Pebax spectrum, which is ascribed to the Si—O stretching. This bound confirms the existence of nanoclay in Pebax matrix.[12] The clay bands at 1047, 464, 627, and 523 cm^{-1} had low intensities, probably due to the low clay content. So the membrane prepared with the higher clay content (10 wt %) showed these characteristics bands with increased intensities. As it is obvious, the O—H band of clay was almost disappeared in MMM samples. It can be said that higher molar mass of polymer hinders O—H band stretching.[26] Another reason can be attributed to the connection (hydrogen bonding) between PA block of Pebax and partially hydrated silicates.[23]

SEM Analysis

FESEM and SEM were used to investigate the morphology of clay particles, surface and cross-section morphology of the membranes, the extent of the polymer–filler adhesion, and distribution of the filler nanoplates inside the polymer matrix. These properties strongly affect the MMMs performance.[4,6,17]

Figure 5 presents the morphology of clay particles clearly. As it is obvious, this plate like structure includes sheets that are bounded with van der Waals forces.[11] With the arrival of polymer chains within these layers that are stuck together by the electrostatic forces, they will separate and disperse in the presence of polymer chains.[14]

Figure 6(a–c) shows surface and cross-section morphology of neat Pebax membrane. As expected the membrane is dense, symmetric, and uniform. The probable defects are related to freezing and fracturing of the membrane in the liquid

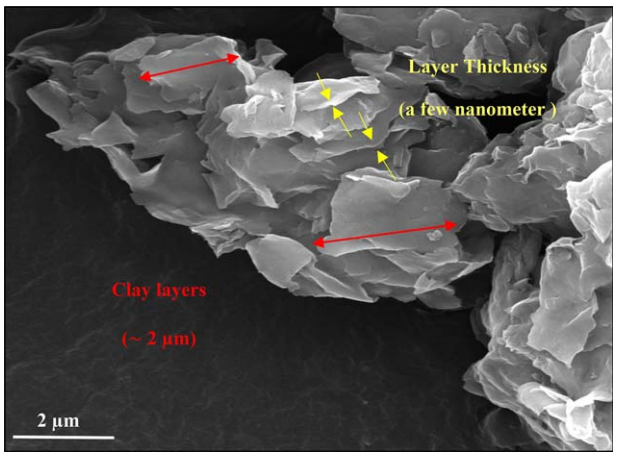

Figure 5. FESEM image of pure clay particles. [Color figure can be viewed at wileyonlinelibrary.com]

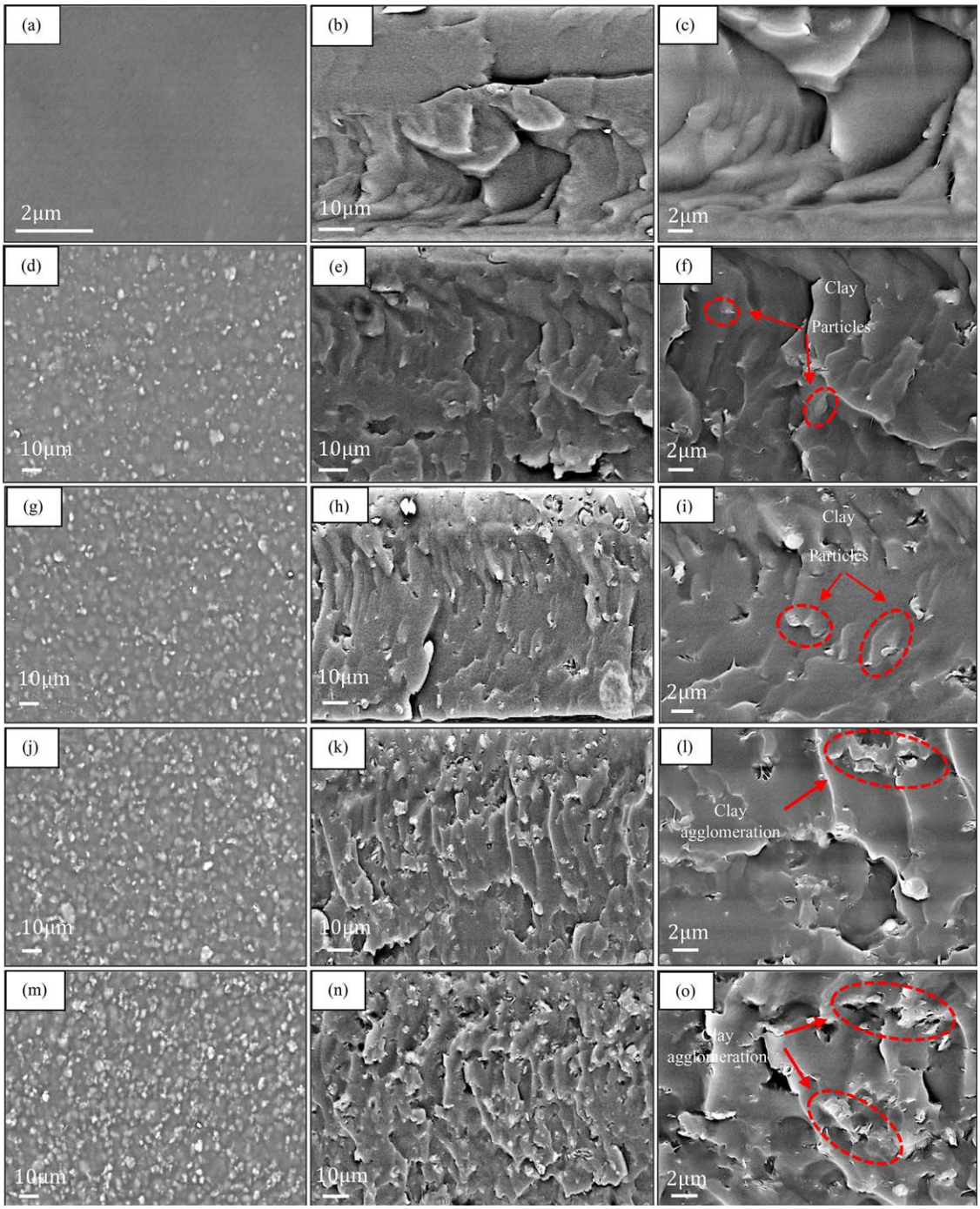

Figure 6. SEM images of the surface (a,d,g,j,m), cross-section at low magnification (b,e,h,k,n), and cross-section at high magnification (c,f,i,l,o) of 0, 2, 4, 6, and 10 wt % Cloisite15A/Pebax2533 MMMs, respectively. [Color figure can be viewed at wileyonlinelibrary.com]

nitrogen.[27] Figure 6 also represents the effect of different loadings of Cloisite15A on the MMMs morphology. As can be seen the surface morphology changes according to the clay loading from relatively smooth surface indicating homogenous dispersion of organoclay in the polymer matrix [Figure 6(e)] to a rougher morphology in higher loading which indicates the presence of some microscale fillers (agglomeration of individual silicate layers) [Figure 6(m)].[8,9,17] Also, from the cross images [Figure 6(e–n)], it can be seen that there is an excellent adhesion and also a high degree of compatibility between the filler particles and the polymer matrix because of the presence of ammonium functional group (dimethyl dehydrogenated tallow quaternary ammonium) in the Cloisite15A interlayers. As a result of the proper adhesion, there is no void formation.[3] Furthermore, hydrophobicity of both phases and flexible rubbery chain mobility of Pebax are other factors for this success.[28,29] Figure 6 also shows that the inorganic particles are dispersed uniformly throughout the polymer matrix in lower loadings,

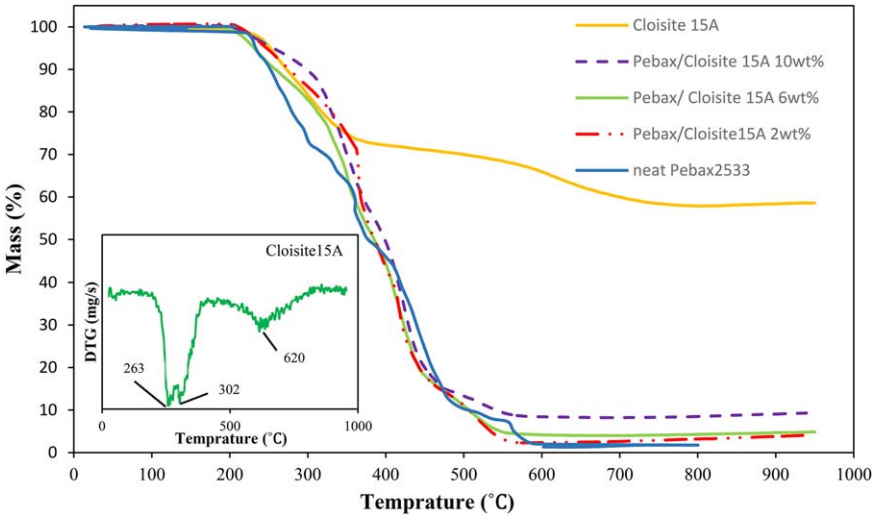

Figure 7. Thermal degradation of Cloisite15A clay and prepared samples. [Color figure can be viewed at wileyonlinelibrary.com]

while by increasing the filler loading, the contacts among the particles are increased which results in particle agglomeration.[3]

TGA Analysis

According to the TGA and DTG [Derivative thermo-gravimetric (−dm/dt)] curves (Figure 7), there are three mass loss stages for Cloisite15A at 263, 302, and 620 °C that are related to functional group decomposition. Generally, there are three possible forms for the functionalize group sitting on clay mineral layers: (1) at the interlayer space, (2) at the external surface, and (3) at the edges of the clay layers. The mass loss occurred at the first peak is attributed to the decomposition of intercalated organic groups trapped into the OMMT structure. Also, the decomposition occurring at the second region is related to the loss of the organic groups, i.e., tallow species grafted onto Si—OH and Al—OH groups, which were covalently bonded to the surface of the clay. This type of modification provides higher thermal stability due to the high stability of covalent bonding. The third major mass loss in the range of the analysis (peak at 620 °C) was associated with the dehydroxylation of structural Al—OH groups of OMMT.[3]

The TGA curves of the MMMs show that there was no loss of mass up to around 200 °C indicating that the casting solvent was not trapped in the polymer matrix or nanoparticle structures.[18] By adding of nanoplates to the matrix, the initial degradation of all MMMs almost remained unchanged.[30] On the other hand, for higher clay loading (10 wt %), in the presence of clay, the onset of mass loss in the nanocomposites occurs at a higher temperature than that of neat polymer (20–30 °C).[15] Figure 7 also illustrates that residual mass of all kinds of MMMs was increased by increasing the clay loading. The residual mass of MMM containing 10 wt % clay was larger than that of others due to high thermal resistance of clay to other MMMs.[30]

These results implied that stability of organoclay, the amount of organoclay, and the relative degree of exfoliation could directly affect the thermal stability of MMMs.[30] On the other hand, it can be said that such thermal degradation was well above the normal operating temperature of some processes.[14,21]

Tensile Test

Tensile strength and elongation at break are two important parameters to describe the mechanical properties of polymeric membranes. The maximum stress at the material can endure under uniaxial tensile loading is defined as the strength which is related to the efficacy of stress transfer between matrix and fillers for micro- and nanocomposites. Filler size, filler loading, and the interfacial strength of filler/matrix are factors that affect the composite strength significantly.[31]

Tensile test was evaluated to study the effect of clay incorporation on the mechanical properties of Pebax/Cloisite15A MMM. The results are reported in Table II and Figure 8. As mentioned before, Pebax2533 is a thermoplastic elastomer with 80% of flexible polyether segments. So that the fabricated membranes were flexible dense films with sufficient mechanical resistance to be handled without difficulties.[18,20] Addition of impermeable particles in this flexible segment lead to reduction in tensile strength of prepared MMMs.[20] As can be seen, with the increase in clay dosage, the tensile strength at break decreased from19 MPa for neat membrane to 15 MPa for Pebax/Cloisite15A-10 wt %. Elongation at break also decreased from 1067% for neat membrane to 784% for Pebax/Cloisite15A-10 wt % MMM. Nevertheless, the mechanical strength maintained in the acceptable limit to withstand the operating conditions.[21] Several

Table II. Mechanical Properties of Samples at Different Clay Loadings

Sample	Tensile strength (MPa)	Elongation at break (%)
Neat Pebax 2533	20 ± 1	1067 ± 65
Pebax/Cloisite15A 2 wt %	18 ± 1	1008 ± 59
Pebax/Cloisite15A 6 wt %	16 ± 3	881 ± 74
Pebax/Cloisite15A 10 wt %	15 ± 2	784 ± 170

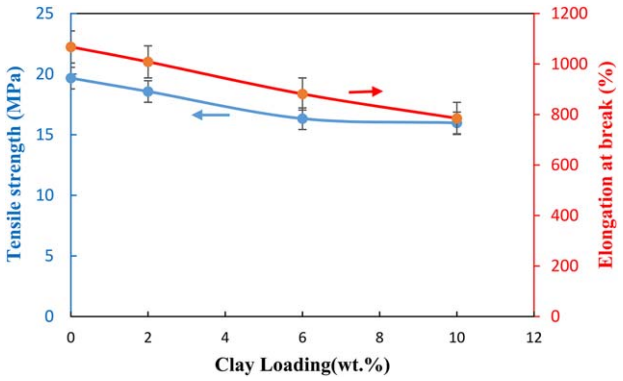

Figure 8. Mechanical properties of prepared samples. [Color figure can be viewed at wileyonlinelibrary.com]

possible reasons can be reliable for this decrease. First of all, higher clay loading can make material frangible.[26] Besides this effect, in higher clay loadings, the micron-sized particles are made because of intercalation or agglomeration of clay particles. This intercalation structure resulting to decrease in aspect ratio of clay platelets leads to weak adhesion between polymer matrix and clay, causing lower tensile strength. On the other hand, filler–filler interaction resulted in agglomeration that may reduce tensile strength of the nanocomposites, due to local stress concentration. Similar results were found by several previous researchers.[31–33] Elongation and expansion of the samples is limited due to created weak sites caused by agglomeration of particles which occurs at high loadings.[34]

Gas Permeation Study

The gas permeation tests were carried out in a constant pressure setup at 2, 4, and 6 bar. Table III depicts the performance of some neat Pebax2533 based MMMs for different gases permeability that reported in the literature for the past decade.

Generally for Pebax 2533, comparison of reported studies in literature is difficult because membrane preparation and permeation test conditions are not identical.[35] Obviously, there was significant differences between permeability values measured in this study and those reported in the literature, especially for nitrogen and hydrogen. This lower permeability can be attributed to the polymer structure. Investigation of solid state structure–property behavior of Pebax series indicates that Pebax polymers are very complex material consisting of complete different phase in nature.[18,36,37] In addition to the different phases, also interphase could behave as a semi-crystalline or a liquid-like phase, may significantly take part in the gas permeation. The reduced mobility and the chain orientation in semi-ordered interphases due to stiff and ordered crystallites would cause the reduction in polymer permeability.[18,37] Factors like thermal and process history, preparation, and polymerization method have also important role on the Pebax2533 morphology and permeability.[36]

In the procedure employed for membrane preparation in this study, the drying step of neat membranes was carried out very slowly in a saturated shield resulting lower evaporation rate of the solvent. This well controlled drying process actually caused the polymer chains to arrange uniformly and for interphase zones to form as a semi-crystalline phase. So that, a higher crystallinity of the polymer and the lower gas permeabilities were obtained.[18] It should be stated that the gas transport through polyether block polyamide, such as Pebax2533 dense films, obeys the solution-diffusion mechanism. Two important factors in this mechanism are solubility (S) and diffusivity (D). The solubility parameter is related to chemical interactions between permeant molecules and polar groups of the copolymer.[20] Meanwhile diffusion coefficient is a kinetic parameter depending on the nature of polymer, penetrant dynamics, and penetrant size.[38] It is also largely determined by polymer chains mobility and to their packing density or free volume that allow the permeant molecules to move.[20]

As said before, Pebax block copolymers are thermoplastic elastomers made of two parts. A rigid polyamide segment that provides mechanical stability of the membrane material and a flexible polyether, either poly(ethylene oxide) or poly(tetra methylene oxide) amorphous segment that is the main gas pass way. Ethylene oxide (EO) units have polar ether group which has high affinity to polar gases (CO_2) resulting a high CO_2 permeability.[19]

H_2 has a smaller kinetic diameter than CO_2, causing more diffusivity for H_2. But as a result of very high solubility of CO_2 in Pebax polymer, there is a reverse selectivity for CO_2/H_2 indicating that in Pebax there is a "solubility controlled" transport.[20]

On the other hand, the mechanism of mass transport of gases permeating in a nanocomposite is similar to that in a semicrystalline polymer. In these cases, the nanocomposite is considered

Table III. Literature Reports for Single Gas Permeabilities (Barrer) of Pebax2533

References	H_2	N_2	CH_4	CO_2	Test conditions
Nafisi and Hagg[19]	—	10	42	351	2 bar and 25 °C
Bernardo *et al.*[20]	47	9.1	31	257	1 bar and 25 °C
Rahman *et al.*[35]	43	9	30	226	1 bar and 30 °C
Ehsani and Pakizeh[18]	33	5.65	29	234	2 bar and 20 °C
This study	32.36 ± 1.4	5.62 ± 0.17	28.36 ± 0.49	239.66 ± 0.86	2 bar and 24 °C
	32 ± 0.19	6.45 ± 0.14	28.99 ± 0.39	242.08 ± 2.09	4 bar and 24 °C
	32.16 ± 0.77	6.56 ± 0.14	29.02 ± 0.67	259.31 ± 5.45	6 bar and 24 °C

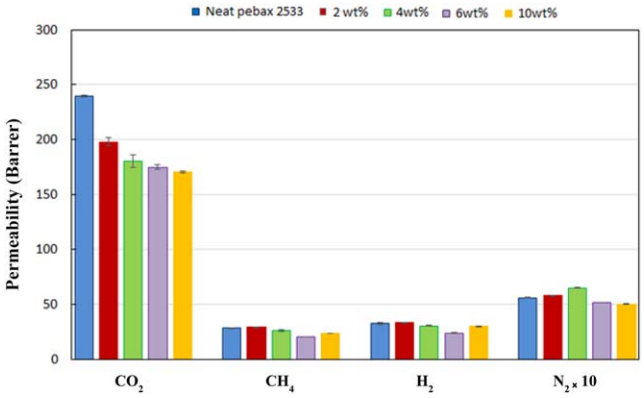

Figure 9. Permeability of CO_2, CH_4, H_2, and N_2 through neat Pebax and MMMs at 2 bar. [Color figure can be viewed at wileyonlinelibrary.com]

to consist of a permeable phase (polymer matrix) where non-permeable nano-platelets are dispersed.[8,13] Tortuosity factor and constraining effect of nanoparticles on the amorphous chains are affecting the diffusion coefficient and gas permeability of nanocomposite materials.[38] Also the permeability of nanocomposites including layered particles is affected by three main factors: volume fraction of the nanoparticles, their relative orientation to the diffusion direction, and their aspect ratio.[8,10,13] The gas transport behavior of nanoclay-reinforced Pebax membranes has been analyzed using CO_2, CH_4, H_2, and N_2 gases and the results were compared with neat Pebax gas permeability which are shown in Figure 9. Also the influence of clay loading on gases permeability can easily be observed in Figure 9.

According to Figure 9, neat pebax2533 polymer shows a relatively high CO_2 permeability that is attributed to the high solubility of CO_2 in the polyether phase.[20] By increasing the nanoplates loading, a decrease of CO_2 permeability is expected due to the reduced solubility caused by polymer matrix volume reduction.[8] Nevertheless, the permeability of gases with more solubility and condensability (i.e., CO_2) will be affected more than others.[8,39]

The presence of clay nanoplates also decreased the adsorption sites of polymer for gas molecules.[39] Another factor is the

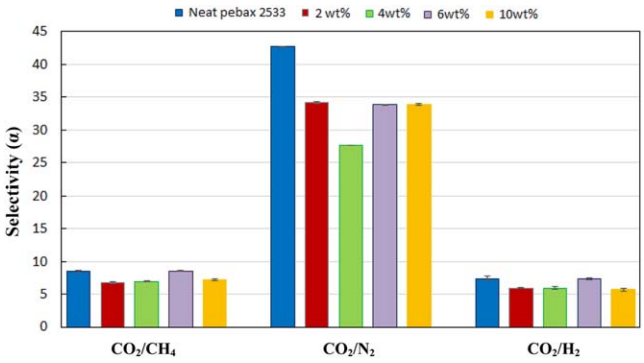

Figure 10. Ideal selectivity plots of neat polymer and MMMs for CO_2/CH_4, CO_2/N_2, and CO_2/H_2 at different loadings in 2 bar. [Color figure can be viewed at wileyonlinelibrary.com]

tortuosity, that is directly related to the shape and the degree of nano-platelets dispersion.[8,13] The dispersion of silicate platelets also has an important role in controlling the polymer–clay nanocomposites structure and gas permeability performances.[39]

Appropriate dispersion of clay particles (exfoliated) increases the tortuosity and diffusion pathway of the molecules while clay agglomeration provides a low resistance pathway for the gas transport by decreasing in the aspect ratio of the nanoparticles.[8] The permeability of CO_2 through MMMs decreased with clay loading that is related to reduction in polymer matrix. Actually increase in the diffusion pathway is also an important factor that have prominent effect in higher loadings. The permeability of CH_4, H_2, and N_2 increased by adding clay (2 wt %), because the addition of a small amount of filler will enhance the accessible free volume in the matrix by interrupting the intrinsic organization of the polymer chains.[24] For sample of 6 wt % clay loading, the permeability of these gases decreased due to increase in diffusion pathway followed by increase in tortuosity.[3,6–9,38–40] Second, exfoliated and intercalated clay layer bundles limit the polymer chain mobility, probably reduce the diffusion coefficient of the gas molecules.[8,39]

In this study, a high degree of compatibility between the organic and inorganic phase is expected due to using modified Mt. However, the increase in clay content has allowed more contacts between the clay particle surface and hindered the dispersion of the clay platelet thus a more intercalated or unmixed system was achieved as previously confirmed by the SEM and XRD analyses.[10] Particles agglomeration at 10 wt % decreases the aspect ratio of the nanoparticles and provides a low resistance pathway for the gas transport.[8,10] Figure 10 illustrates the ideal selectivity of each pair of gases versus clay loading at the pressure of 2 bar. Neat polymer membrane has maximum CO_2 permeability due to more solubility of this gas in polymer matrix resulting maximum CO_2/gas selectivity. Even there is a reverse selectivity about the CO_2/H_2, meaning that solubility of larger molecules is surmount diffusivity of smaller molecules.[20]

However for MMMs, different trend was observed in which by increasing clay loading up to 4 wt % CO_2/CH_4, CO_2/N_2, CO_2/H_2 were decreased. This may be attributed to the reduction of CH_4, N_2, and H_2 permeability due to increasing diffusion pathway and reduction of CO_2 permeability caused by decline of adsorption sites.

Figure 11(a–c) shows the effect of pressure on gases permeability. As shown, the permeability of more condensable and soluble gas (CO_2) increased by increase in pressure from 2 to 6 bar due to CO_2 solubility increment in polymer matrix at all filler loadings. While, CH_4 and H_2 permeabilities were not considerably affected with pressure. For these most diffusion controlled gases, solubility and diffusion coefficient are independent on the pressure.[42,43]

The influence of pressure on gas permeability is affected by important factors such as the gas molecules, the film structure, and the pressure involved.[44] The dependent of permeability to the pressure can be assigned in the forms of $S(P)$ and $D(P)$ according to the solution-diffusion mechanism. For low-

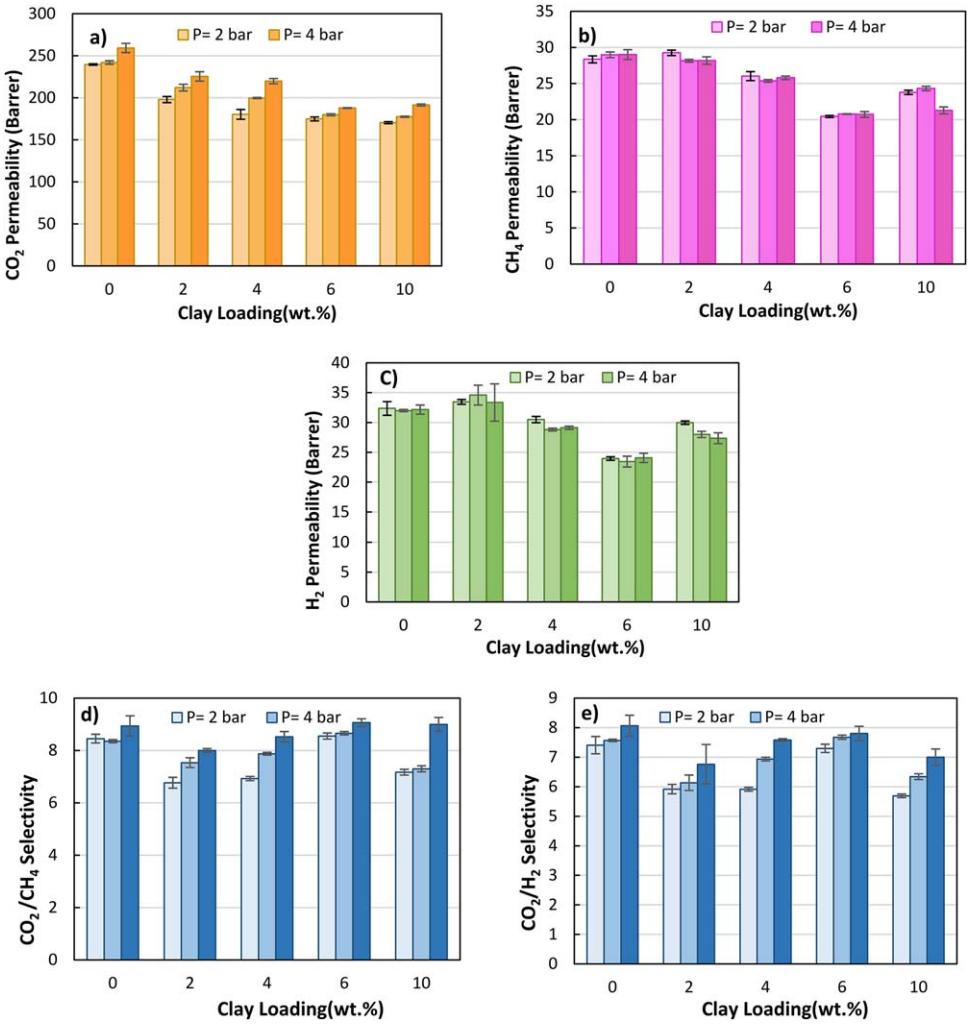

Figure 11. The effect of pressure on (a) CO_2 permeability, (b) CH_4 permeability, (c) H_2 permeability, (d) CO_2/CH_4 ideal selectivity, and (e) CO_2/H_2 ideal selectivity at different clay loadings. [Color figure can be viewed at wileyonlinelibrary.com]

adsorbing penetrants with low condensability, the permeability exhibits little or no change with increasing pressure.[41] In contrast, for high-adsorbing penetrants with high condensability, solubility typically increases with increasing pressure, resulting in increase in permeability coefficients as in the case for CO_2.[42] By the way, some strongly adsorbing penetrants can plasticize the polymer matrix in high concentrations. Plasticization effectively increases the chain spacing mobility and polymer local segmental motion so that the diffusion and permeation coefficients increase with increasing penetrant pressure.[41,42]

Figure 11(d,e) shows CO_2/CH_4 and CO_2/H_2 selectivities at different pressure and clay loadings. For each clay loading, pressure increment enhances the CO_2/CH_4 and CO_2/H_2 selectivities. The highest CO_2/CH_4 selectivity was obtained at all pressures for 6 wt % clay MMM while the highest CO_2/H_2 selectivity was achieved for neat polymer at 6 bar. As can be concluded the ideal selectivities related to CO_2 are increased as a function of pressure. This can be clearly described by considering the single gas permeability variations (solubility for CO_2 and diffusivity for others) with pressure.

CONCLUSIONS

Pebax2533/Cloisite15A MMMs were successfully prepared by solution casting method without void and defect formation at surface or clay/polymer interface due to well controlled casting solution concentration and evaporation conditions. There was an appropriate adhesion between polymer and nanoparticles which were confirmed by several characterization methods. It was concluded that at low loading, clay dispersion occurred as exfoliated-intercalated and at high loading as intercalated-phase separated. CO_2 permeability decreased by specific extent with adding impermeable clay layers due to reduction in gas solubility in polymer matrix. Also no significant increase was observed in CO_2/CH_4 selectivity with the increase in Cloisite15A loading at constant pressure. In contrast, CO_2 permeability increased with pressure increment but permeability of CH_4 and H_2 gases remained nearly

constant. By increasing of pressure from 2 to 6 bar, CO_2/CH_4 permselectivity enhanced for all nanoclay loadings.

REFERENCES

1. Rezakazemi, M.; Amooghin, A. E.; Montazer-Rahmati, M. M.; Ismail, A. F.; Matsuura, T. *Prog. Polym. Sci.* **2014**, *39*, 817.
2. Yi, L. Ph.D. Thesis, National University of Singapore, **2007**.
3. Hashemifard, S. A.; Ismail, A. F.; Matsuura, T. *Chem. Eng. J.* **2011**, *170*, 316.
4. Liang, C.-Y.; Uchytil, P.; Petrychkovych, R.; Lai, Y.-C.; Friess, K.; Sipek, M.; Reddy, M. M.; Suen, S.-Y. A. *Sep. Purif. Technol.* **2012**, *92*, 57.
5. Chung, T.-S.; Jiang, L. Y.; Li, Y.; Kulprathipanja, S. *Prog. Polym. Sci.* **2007**, *32*, 483.
6. Ching, O. P.; Lung, B.; Wong, M. *Appl. Mech. Mater.* **2014**, *625*, 696.
7. Zulhairun, A.; Ismail, A.; Matsuura, T.; Abdullah, M.; Mustafa, A. *Chem. Eng. J.* **2014**, *241*, 495.
8. Wilson, R.; Plivelic, T. S.; Aprem, A. S.; Ranganathaiagh, C.; Kumar, S. A.; Thomas, S. *J. Appl. Polym. Sci.* **2012**, *123*, 3806.
9. Wilson, R.; George, S. M.; Maria, H. J.; Plivelic, T. S.; Kumar, S. A.; Thomas, S. *J. Phys. Chem. C* **2012**, *116*, 20002.
10. Ismail, N.; Ismail, A.; Mustafa, A.; Matsuura, T.; Soga, T.; Nagata, K.; Asaka, T. *Chem. Eng. J.* **2015**, *268*, 371.
11. Ray, S. S. Clay-Containing Polymer Nanocomposites: From Fundamentals to Real Applications. Newnes: Jaddah, **2013**; Chapter 1, p 1.
12. Dehkordi, F. S.; Pakizeh, M.; Namvar-Mahboub, M. *Appl. Clay Sci.* **2015**, *105*, 178.
13. Choudalakis, G.; Gotsis, A. *Eur. Polym. J.* **2009**, *45*, 967.
14. Hafiz, A. A. A. Ph.D. Thesis, The American University in Cairo, **2013**.
15. Muralidharan, M.; Kumar, S. A.; Thomas, S. *J. Membr. Sci.* **2008**, *315*, 147.
16. Villaluenga, J.; Khayet, M.; Lopez-Manchado, M.; Valentin, J.; Seoane, B.; Mengual, J. *Eur. Polym. J.* **2007**, *43*, 1132.
17. Defontaine, G.; Barichard, A.; Letaief, S.; Feng, C.; Matsuura, T.; Detellier, C. *J. Colloid Interface Sci.* **2010**, *343*, 622.
18. Ehsani, A.; Pakizeh, M. *J. Taiwan Inst. Chem. Eng.* **2016**, *66*, 414.
19. Nafisi, V.; Hägg, M.-B. *J. Membr. Sci.* **2014**, *459*, 244.
20. Bernardo, P.; Jansen, J. C.; Bazzarelli, F.; Tasselli, F.; Fuoco, A.; Friess, K.; Izák, P.; Jarmarová, V.; Kačírková, M.; Clarizia, G. *J. Membr. Sci.* **2012**, *97*, 73.
21. Jaafar, J.; Ismail, A. F.; Matsuura, T. *J. Membr. Sci.* **2009**, *345*, 119.
22. Sridhar, S.; Aminabhavi, T.; Mayor, S.; Ramakrishna, M. *Ind. Eng. Chem.* **2007**, *46*, 8144.
23. Kim, J. H.; Lee, Y. M. *J. Membr. Sci.* **2001**, *193*, 209.
24. Liu, S.; Liu, G.; Zhao, X.; Jin, W. *J. Membr. Sci.* **2013**, *446*, 181.
25. Yürüdü, C.; İşçi, S.; Ünlü, C.; Atıcı, O.; Ece, Ö. I.; Güngör, N. *J. Appl. Polym. Sci.* **2006**, *102*, 2315.
26. Anadao, P.; Montes, R. R.; Larocca, N. M.; Pessan, L. A. *Appl. Surf. Sci.* **2013**, *275*, 110.
27. Zhang, Y.; Musselman, I. H.; Ferraris, J. P.; Balkus, K. J. *J. Membr. Sci.* **2008**, *313*, 170.
28. Mahajan, R.; Burns, R.; Schaeffer, M.; Koros, W. J. *J. Appl. Polym. Sci.* **2002**, *86*, 881.
29. Li, T.; Pan, Y.; Peinemann, K.-V.; Lai, Z. *J. Membr. Sci.* **2013**, *425*, 235.
30. Koh, H. C.; Park, J. S.; Jeong, M. A.; Hwang, H. Y.; Hong, Y. T.; Ha, S. Y.; Nam, S. Y. *Desalination* **2008**, *233*, 201.
31. Fu, S.-Y.; Feng, X.-Q.; Lauke, B.; Mai, Y.-W. *Compos. Part B* **2008**, *39*, 933.
32. Wildan, M.; Mohd Ishak, Z. *Int. J. Polym. Sci.* **2013**, *2013*.
33. Lepoittevin, B.; Devalckenaere, M.; Pantoustier, N.; Alexandre, M.; Kubies, D.; Calberg, C.; Jérôme, R.; Dubois, P. *Polymer* **2002**, *43*, 4017.
34. Jaafar, J.; Ismail, A. F.; Matsuura, T.; Nagai, K. *J. Membr. Sci.* **2011**, *382*, 202.
35. Rahman, M. M.; Filiz, V.; Shishatskiy, S.; Abetz, C.; Neumann, S.; Bolmer, S.; Khan, M. M.; Abetz, V. *J. Membr. Sci.* **2013**, *437*, 286.
36. Scholes, C. A.; Bacus, J.; Chen, G. Q.; Tao, W. X.; Li, G.; Qader, A.; Stevens, G. W.; Kentish, S. E. *J. Membr. Sci.* **2012**, *389*, 470.
37. Sheth, J. P.; Xu, J.; Wilkes, G. L. *Polymer* **2003**, *44*, 743.
38. Nguyen, Q. T.; Sublet, J.; Langevin, D.; Chappey, C.; Marais, S.; Valleton, J. M.; Poncin-Epaillard, F. *Membr. Gas Sep.* **2010**, *9*, 255.
39. Ryu, S. H.; Chang, Y.-W. *Polym. Bull.* **2005**, *55*, 385.
40. Goh, P. S.; Ismail, A. F.; Sanip, S. M.; Ng, B. C.; Aziz, M. *Sep. Purif. Technol.* **2011**, *81*, 243.
41. Bhole, Y. S.; Wanjale, S. D.; Kharul, U. K.; Jog, J. P. *J. Membr. Sci.* **2007**, *306*, 277.
42. Freeman, B.; Yampolskii, Y.; Pinnau, I., Eds. Materials Science of Membranes for Gas and Vapor Separation; Wiley: West Sussex, U.K., **2006**.
43. Lin, H.; Freeman, B. D. *J. Membr. Sci.* **2004**, *239*, 105.
44. Pye, D.; Hoehn, H.; Panar, M. *J. Appl. Polym. Sci.* **1976**, *20*, 1921.